

Prompt-fission γ -ray spectral characteristics from $^{239}\text{Pu}(n_{\text{th}},f)$ A. Gatera,^{1,2} T. Belgia,³ W. Geerts,¹ A. Göök,¹ F.-J. Hamsch,¹ M. Lebois,⁴ B. Maróti,³ A. Moens,¹ A. Oberstedt,⁵ S. Oberstedt,^{1,*} F. Postelt,⁶ L. Qi,⁴ L. Szentmiklósi,³ G. Sibbens,¹ D. Vanleeuw,¹ M. Vidali,¹ and F. Zeiser⁷¹European Commission, Joint Research Centre, Directorate G, Retieseweg 111, 2440 Geel, Belgium²Ghent University, Department of Physics and Astronomy, Proeftuinstraat 86, 9000 Ghent, Belgium³Centre for Energy Research, Hungarian Academy of Sciences, Nuclear Analysis and Radiography Department, 1525 Budapest, Hungary⁴Institut de Physique Nucléaire Orsay (IPN-Orsay), 91406 Orsay, France⁵Extreme Light Infrastructure-Nuclear Physics (ELI-NP)/Horia Hulubei National Institute for Physics and Nuclear Engineering (IFIN-HH), 077125 Bucharest-Magurele, Romania⁶Hamburg University, Department of Physics, Hamburg, Germany⁷University of Oslo, Department of Physics, Oslo, Norway

(Received 9 March 2017; published 13 June 2017)

In this paper we present new results for prompt fission γ -ray spectral characteristics from the thermal neutron induced fission of $^{240}\text{Pu}^*$. The measured spectra were unfolded by using the detectors' response functions, simulated with GEANT4. We obtained in average per fission a γ -ray multiplicity $\bar{M}_\gamma = (7.35 \pm 0.12)$, a mean photon energy $\bar{\epsilon}_\gamma = (0.85 \pm 0.02)$ MeV, and an average total energy released in fission $\bar{E}_{\gamma,\text{tot}} = (6.27 \pm 0.11)$ MeV. Our results are in good agreement with historical data measured in the 1970s by Verbinski *et al.* and results from recent calculations in the framework of Monte Carlo Hauser–Feshbach models. Our measured average total energy is slightly smaller than the one deduced previously and present in evaluated data. From this we conclude that the $^{239}\text{Pu}(n_{\text{th}},f)$ reaction may be ruled out as possible source of γ heating underestimation, when compared with benchmark calculations based on existing nuclear data.

DOI: [10.1103/PhysRevC.95.064609](https://doi.org/10.1103/PhysRevC.95.064609)**I. INTRODUCTION**

Recent benchmark exercises on nuclear reactors have revealed an underestimation of prompt γ heating by 10% to 28% for ^{235}U and ^{239}Pu [1]. This has motivated a revival for measurements of prompt-fission γ -ray spectral (PFGS) characteristics, and international efforts have been put into improving the accuracy of data since the latest results dated from the 1970s. Our team measured several fissioning systems including $^{252}\text{Cf}(sf)$ [2,3], $^{235}\text{U}(n_{\text{th}},f)$ [4], $^{241}\text{Pu}(n_{\text{th}},f)$ [5], and $^{240,242}\text{Pu}(sf)$ [6] by using state-of-the-art cerium-doped lanthanum bromide detectors ($\text{LaBr}_3:\text{Ce}$). The detectors were chosen for their superior energy and timing resolution compared with widely used thallium-doped sodium iodide (NaI) or barium fluoride (BaF_2) scintillation detectors [7].

The previous measurements showed little deviation [8] from the evaluated data based on the measurements by Verbinski *et al.* in the 1970s [9]. The reaction $^{239}\text{Pu}(n,f)$ is the second of the two candidates on the High Priority Request List (HPRL) published by the OECD/NEA, beside $^{235}\text{U}(n_{\text{th}},f)$ [4], aiming to improve the precision of PFGS characteristics to an uncertainty lower than 7.5% [1]. A big challenge in the $^{239}\text{Pu}(n_{\text{th}},f)$ reaction measurement is the high specific alpha activity of 2 MBq/mg.

In the following sections we describe our experimental setup, our data analysis with the particular scope on how to deal with the high α activity and the unfolding process of our spectra. Then our results will be shown and compared with existing experimental data and model calculations.

II. EXPERIMENTAL SETUP AND DATA ANALYSIS

The experiment took place at the 10 MW research reactor of the Budapest Neutron Centre in Hungary. The beam line provided an equivalent thermal-neutron flux of 5×10^7 neutrons/s. A 430 μg high-purity plutonium target (99.97% of ^{239}Pu) was used. It generated around one million alpha particles/s and 40 thousand fission events/s.

As fission detector we used a Frisch-grid ionization chamber (FGIC). This detector does not suffer from radiation damage and covers a solid angle of 2π giving an efficiency for detecting fissions close to 100%. To cope with the high α activity we operated the FGIC with a counting gas that has a high electron mobility. We chose a mixture of Argon- CF_4 (10%). This counting gas has also a higher stopping power allowing a more compact design and, as a consequence, leading to shorter signal traces. In this experiment we reached an electron drift time of 150 ns for a cathode-grid distance of 20 mm, and the cathode signal for fission fragments was about 200 ns wide.

The ^{239}Pu target was placed in the cathode center of the FGIC. The cathode signal was used as fission trigger and a counter registered the number of triggers. The fission fragments' angular distribution was extracted from the grid signal, and the anode measured their energies. More details about the FGIC signal treatment can be found in Ref. [10].

*stephan.oberstedt@ec.europa.eu

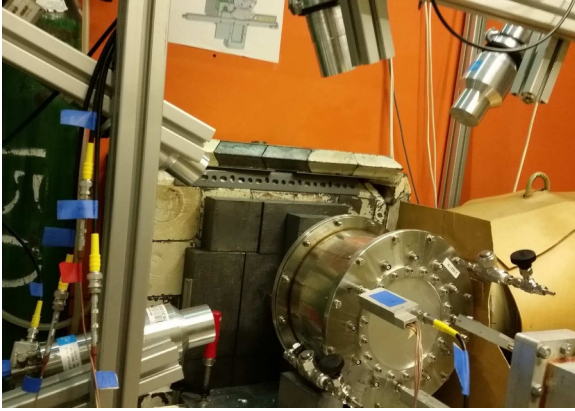


FIG. 1. Picture of the prompt-fission γ -ray measurement setup in Budapest: Four $\text{LaBr}_3:\text{Ce}$ detectors of size (diameter \times length) $5.08 \text{ cm} \times 5.08 \text{ cm}$, were placed at 90 degrees relative to the neutron beam axis at a distance of 36 cm from the center of the chamber where the plutonium sample was mounted in the center of the cathode.

Four $\text{LaBr}_3:\text{Ce}$ detectors were placed in the target plane at a distance of 36 cm from the target center. A picture of the experimental setup is shown in Fig. 1.

The data-acquisition system consisted of seven channels of 14 bit wave-form digitizers with a sampling rate of 400 MS/s. The system was triggered whenever a γ ray was detected within a window of 300 ns following the fission trigger. In that case, all the signal traces were digitized and saved for offline analysis. We acquired on average 2000 coincidences/s.

The off-line analysis is done using digital signal processing (DSP) techniques and the different energy and timing spectra are saved to a ROOT tree [11]. From the processed data, relevant fission events and relevant prompt-fission γ rays are selected.

A. Alpha and pileup rejection

In case of a highly alpha-active sample and high fission rate, the cathode of the ionization chamber that gives the fission trigger is also triggered by a pileup of either α particles or fission fragments. Counting all events as total number of fissions would induce a systematic error in all the different spectral characteristics that are normalized to the total number of fissions. To optimize rejection of pileup events, we used two techniques to make sure that those parasitic events can be discriminated from clean fission events.

In addition to the use of a fast counting gas, we apply a pileup rejection algorithm based on signal length. We calculate for every trace the length of the cathode signal above a fixed threshold, and as this length varies with the number of present signals in the traces, it allows us to identify pileup events. The limit of the method is reached when the signals are sitting on top of each other but in that case they can, in all problematic cases, be discriminated by their accumulated pulse height. Some α -fission pileups cannot be isolated, but they are not an issue when we are exclusively interested in the number of fissions. The grid pulse height, which is proportional to cosine of the emission angle, versus the anode pulse height,

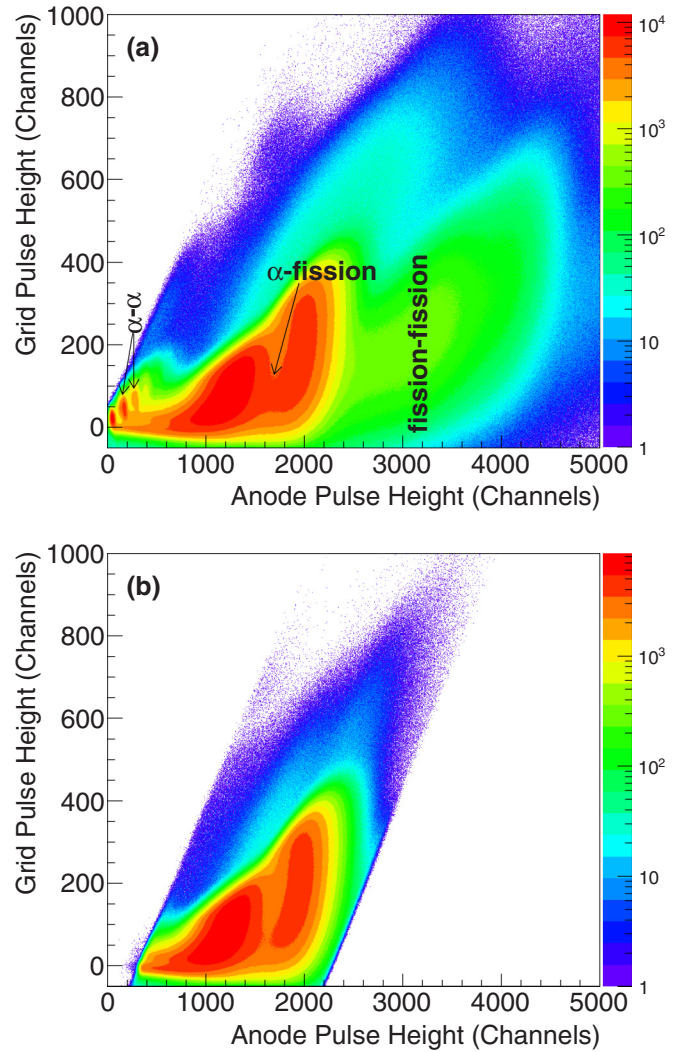


FIG. 2. Fission-fragment distribution (a) before and (b) after applying α and pileup rejection to the raw data. The anode pulse height is proportional to the fragment's energy and the grid pulse height to its emission angle. In the upper plot (a) we can see multiple α -particle pileups to the left, α -fission-fragment pileups that are obvious in the center of the two fission fragments, blurring the separation of the heavy and the light fragments, and to the right an extra fission-fission pileup distribution that resembles the original one. In the bottom plot (b), all the α -particle pileups and fission-fission pileups are properly filtered. A fraction of α -fission-fragment pileups remains in the data, but they do not affect the total fission count.

proportional to the fragment's energy, is depicted in Fig. 2(a) before and Fig. 2(b) after the filtering algorithm has been applied. Only the events after filtering count as fission events for the rest of the analysis. More details about the FGIC's signals treatment can be found in Ref. [10].

B. Time-of-flight discrimination

Figure 3 shows the time-of-flight (TOF) spectrum of γ rays based on the fission timing (time zero) as a function of γ -ray energy. It shows a prompt peak, followed by a γ -ray distribution generated by prompt neutrons, where a few γ lines,

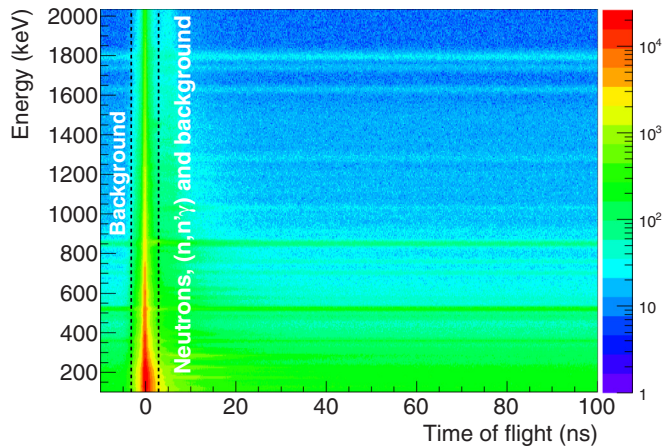


FIG. 3. Time-of-flight (TOF) spectra for different γ -ray energies. Time 0 is the fission trigger timing. The region on the far left before the fission trigger is pure background and is subtracted from the rest of the spectrum. The FWHM of the prompt-fission γ -ray peak is around 1.20 ns, and we consider most of prompt γ rays to be included in the interval $[-3, 3]$ ns which stops right before the neutrons reach the detector. A cut on this region after background subtraction constitutes our measured prompt-fission γ -ray spectrum. To the right of the prompt peak, we can see a few $(n, n'\gamma)$ lines from all the materials surrounding the detectors. The iron from the cathode is too close to the target and when looking closely at the distribution around 847 keV, some of its neutron-induced γ rays are slightly in the prompt window (easier to see in Fig. 4). This yield is removed during the unfolding process.

resulting from neutrons inelastically scattered in materials surrounding the detector, can be seen (yellow horizontal lines on the right of the prompt peak). A continuous background is visible as well. We determined its contribution from the time region before the fission trigger, i.e., left from the prompt peak in Fig. 3, and subtracted it from the spectrum obtained from the prompt region.

The prompt timing distribution has a full width at half maximum (FWHM) of 1.20(5) ns. The width of the prompt window was defined to stop right before the prompt neutron contribution reaches the detector. We also made sure to obtain the same relative width, with respect to the FWHM, as Verbinski *et al.* [9]. They reported a prompt interval of ± 10 ns for a FWHM of 4 ns. The same ratio gives in our case a time cut set to ± 3 ns around zero.

Once the resulting prompt γ -ray spectrum was obtained, it was unfolded by using a GEANT4 [12] Monte Carlo simulated response function. The simulated response function of $\text{LaBr}_3\text{:Ce}$ detectors is very sensitive to the detector's surroundings, especially at low energies around the backscatter peak region (below 300 keV) [13]. The simulations needed to be validated every time that the measurement setup was modified by comparing measured and simulated responses for well-calibrated γ -ray energies.

One of our four detectors showed an efficiency inconsistency at high energies, so we discarded it from further analysis. The remaining three detectors give measured prompt-fission γ -ray spectra (PFGS) that agree very well with each other,

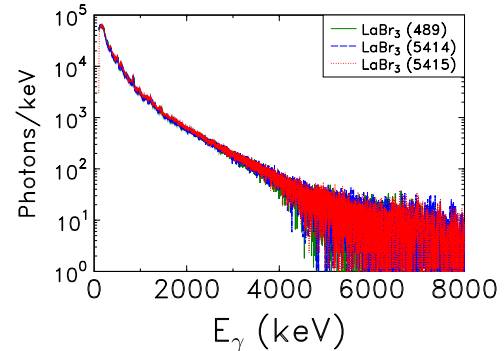


FIG. 4. PFGS as measured before the unfolding process for the three lanthanum bromide detectors, which are labeled by their serial numbers. $\text{LaBr}5415$ has a slightly higher yield compared with the two other detectors. It could be explained by a shift in distance to target of 2 mm, which was the estimated precision of our distance measurements.

as shown in Fig. 4. Small shifts in peak position can be observed because of a bin size smaller than the detectors' energy resolution in the order of 3% at 667 keV [7].

III. RESULTS AND DISCUSSION

A. The unfolded spectra

The purpose of a response function simulation is to obtain a measured spectrum specific to the detector and the measurement environment for a monoenergetic γ ray of a given energy. We simulated 300 energies in the range from 100 keV to 10 MeV with a spacing depending on the detector's energy resolution function. A weighted sum of the simulated spectra was used to fit the measured spectra given in Fig. 4.

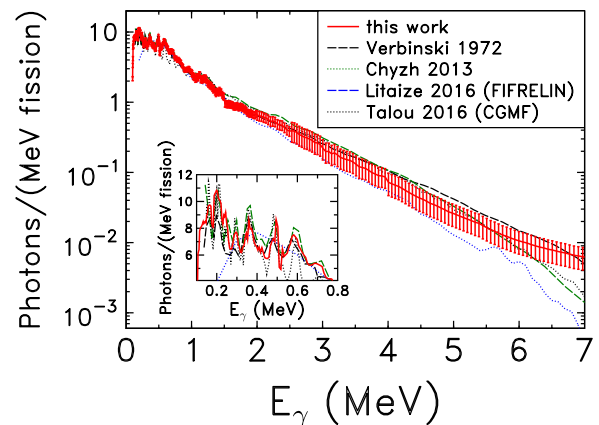


FIG. 5. Overview of PFGS from the reaction $^{239}\text{Pu}(n, f)$: the spectrum obtained in this work represents an average from three detectors after unfolding the response functions. Above ≈ 300 keV the agreement with the measured data from Verbinski [9] and Chyzh [14] and with the calculated spectra by Litaize [15] and Talou [16] is rather good considering the error bars, below the spectrum from Ref. [14] deviates, which has been observed earlier [3]. The inset shows focus on the low-energy structure and shows how well the different calculations are able to predict it.

TABLE I. Summary of prompt-fission γ -ray characteristics for the thermal- and slow-neutron-induced fission on ^{239}Pu . Experimental results from this work for the average γ -ray multiplicity \bar{M}_γ , the average energy ϵ_γ , and the total energy $E_{\gamma,\text{tot}}$, obtained with all three detectors, are given and the covered energy range is indicated. As already seen in Fig. 4, LaBr₃:Ce (5415) yields a slightly higher average energy than the two other detectors. Spectrum characteristics obtained after summing the three measured spectra before unfolding the resulting spectrum are given, too. Our results are compared with historical data from Verbinski *et al.* [9] and Pleasonton [17] as well as with more recent data from Chyzh *et al.* [14] and Ullmann *et al.* [18] obtained from epithermal neutron-induced fission, with Monte Carlo Hauser–Freshback calculations from both Litaize *et al.* [15] and Talou *et al.* [16], and the evaluated nuclear data files in ENDF/B-VII.1 [19]. To allow proper comparison we also give the experimental timing resolution (FWHM) and the selected time window Δt .

Results	Detector	Diameter \times length (cm \times cm)	FWHM (ns)	Δt (ns)	\bar{M}_γ (per fission)	ϵ_γ (MeV)	$E_{\gamma,\text{tot}}$ (MeV)	Energy range (MeV)
This work	LaBr ₃ :Ce (Q489)	5.08 \times 5.08	1.2	± 3	7.27 \pm 0.11	0.85 \pm 0.02	6.18 \pm 0.10	0.1–7.0
This work	LaBr ₃ :Ce (5414)	5.08 \times 5.08	1.2	± 3	7.35 \pm 0.11	0.84 \pm 0.02	6.17 \pm 0.09	0.1–7.0
This work	LaBr ₃ :Ce (5415)	5.08 \times 5.08	1.2	± 3	7.26 \pm 0.11	0.88 \pm 0.02	6.42 \pm 0.10	0.1–7.0
This work	LaBr ₃ :Ce	Summed spectra	1.2	± 3	7.35 \pm 0.12	0.85 \pm 0.02	6.27 \pm 0.11	0.1–7.0
Verbinski [9]	NaI:Tl	5.85 \times 15.2	4	± 10	7.23 \pm 0.22	0.94 \pm 0.05	6.81 \pm 0.30	0.14–10.0
Pleasonton [17]	NaI:Tl	12.7 \times 10.2	5.3	± 5	6.88 \pm 0.35	0.98 \pm 0.07	6.73 \pm 0.35	0.12–6.31
Chyzh [14]	DANCE calorimeter		1.7	± 4	7.93	1.00	7.94	0.2–9.5
Ullmann [18]	DANCE calorimeter		2	± 5	7.15 \pm 0.09	1.04 \pm 0.02	7.46 \pm 0.06	0.15–10.0
Litaize [15]	Calculation			10	7.70	0.92	7.10	0.14–10.0
Talou [16]	Calculation			10	7.22	0.91	6.55	0.14–10.0
ENDF/B-VII.1 [19]	Evaluation				7.78	0.87	6.73	0.05–8.0

The obtained result is the number of γ rays emitted in each energy bin to build up the measured spectrum, which leads us to the emitted spectrum. Details about the unfolding process can be found in previous publications; see, e.g., Ref. [2].

Considering the low statistics above 5 MeV, an exponential fit is applied to the data, which gives satisfactory results up to 7 MeV. Above that energy our fit proved unreliable, but it is not an issue, since the region above 7 MeV has very little impact on the average values. Verbinski *et al.* [9] calculated the emission yield in the interval 7–10 MeV to contribute to the total energy for less than 0.3% which is an order of magnitude lower than our uncertainty; this result was corroborated in Ref. [4]. The uncertainties of the fit parameters contribute to the systematic uncertainty of the photon yield in each energy bin.

In Fig. 5 we compare the shape of the obtained emission spectrum, averaged over the three remaining detectors, with different experimental data [9,14] and results from model calculations [15,16].

B. Average spectral characteristics

Characteristic parameters for prompt-fission γ -ray emission, like the average number of photons per fission, \bar{M}_γ , the average total energy per fission, $E_{\gamma,\text{tot}}$, and the mean photon energy, ϵ_γ , were obtained according to

$$\bar{M}_\gamma = \int N_\gamma(E_\gamma) dE_\gamma, \quad (1)$$

$$E_{\gamma,\text{tot}} = \int E_\gamma \times N_\gamma(E_\gamma) dE_\gamma, \quad (2)$$

$$\epsilon_\gamma = E_{\gamma,\text{tot}} / \bar{M}_\gamma, \quad (3)$$

with $N_\gamma(E_\gamma)$ denoting the spectra depicted in Fig. 5. The lower energy limit was chosen as 100 keV for all detectors, since the low-energy thresholds in this experiment were just below. The characteristic parameters were determined for each detector by replacing the integrals above by sums and average values, weighted with the individual uncertainties, were calculated.

As can be seen in Table I, our results show a good overall agreement with other published results. Our multiplicity agrees with Verbinski's value [9] within the error bars, but because we calculate a lower mean energy, as was the case for $^{252}\text{Cf}(sf)$ [2], $^{235}\text{U}(n_{\text{th}}, f)$ [4], and $^{241}\text{Pu}(n_{\text{th}}, f)$ [5], we obtain a lower average total energy per fission. Recent calculations suggest that the chosen experimental coincidence window can change the average total energy by up to 5% [16].

Table II shows the absolute contribution to the total uncertainties of the different parameters. The statistical uncertainties are very low due to the 3.05×10^8 fission- γ -ray coincidences

TABLE II. Detailed contributions to the total uncertainties of prompt-fission γ -ray characteristics given in Table I. The two first lines show absolute contributions to the total uncertainties, and the three last lines detail relative contributions to the systematic uncertainties.

Type of uncertainty	\bar{M}_γ (fission ⁻¹)	ϵ_γ (MeV)	$E_{\gamma,\text{tot}}$ (MeV)
Statistical (fission, simulation, γ ray)	0.004	0.002	0.018
Systematics	0.109	0.017	0.083
(i) Simulation (setup, cross section)	84.2%	76.4%	70.5%
(ii) Energy calibration		1.6%	2.2%
(iii) Fitting detector response	15.8%	22.0%	27.3%

measured and the 1.0×10^8 events simulated per energy. The main part of our systematic uncertainties comes from the simulated response functions and cross sections. The response of the three identical detectors in the present setup appeared very similar. Therefore, the same energy-dependent simulated response was applied to the three detectors. The deviation of the simulated to the measured response to reference γ -ray sources are treated as systematic uncertainties.

IV. CONCLUSIONS

New PFGS characteristics for $^{239}\text{Pu}(n, f)$ were measured with high statistical accuracy and reduced error margins. Digital algorithms were used to process the data and the measured spectra were unfolded by using Monte Carlo simulated response functions, with extra focus on a faithful modeling of the experimental setup.

Our results are in good agreement, within uncertainties, with other published results. The spectral shape resembles perfectly the previously measured ones and fits very well to the calculations. We report a slightly smaller total energy. This

may be at least partially explained by our shorter time window after fission that reduces the amount of isomeric decay γ rays included in the results.

Based on the results presented here and all the other fissioning systems that we have remeasured so far, we have found quite small deviations from the evaluated nuclear data in ENDF/B-VII.1, too small to explain the observed shortcomings with respect to benchmark calculations. We think that this is proof enough to exclude thermal-neutron-induced fission from the list of possible causes to the underestimation of γ heating. Fast-neutron-induced fission is now also being investigated [20].

ACKNOWLEDGMENTS

The authors are indebted to the CHANDA Program (Agreement No. 605203) for funding the experiment in Budapest. Special thanks to O. Litaize and P. Talou for valuable discussions and for their interest in this work. The European Commission is gratefully acknowledged for providing Ph.D. fellowship program support to A. Gatera.

-
- [1] Nuclear Data High Priority Request List of the NEA (Req. ID: H.3, H.4), <http://www.nea.fr/html/dbdata/hprl/hprlview.pl?ID=421> and <http://www.nea.fr/html/dbdata/hprl/hprlview.pl?ID=422>.
- [2] R. Billnert, F.-J. Hamsch, A. Oberstedt, and S. Oberstedt, *Phys. Rev. C* **87**, 024601 (2013).
- [3] A. Oberstedt, R. Billnert, F.-J. Hamsch, and S. Oberstedt, *Phys. Rev. C* **92**, 014618 (2015).
- [4] A. Oberstedt, T. Belgya, R. Billnert, R. Borcea, T. Bryś, W. Geerts, A. Göök, F.-J. Hamsch, Z. Kis, T. Martinez, S. Oberstedt, L. Szentmiklosi, K. Takács, and M. Vidali, *Phys. Rev. C* **87**, 051602(R) (2013).
- [5] S. Oberstedt, R. Billnert, T. Belgya, T. Bryś, W. Geerts, C. Guerrero, F.-J. Hamsch, Z. Kis, A. Moens, A. Oberstedt, G. Sibbens, L. Szentmiklosi, D. Vanleeuw, and M. Vidali, *Phys. Rev. C* **90**, 024618 (2014).
- [6] S. Oberstedt, A. Oberstedt, A. Gatera, A. Göök, F.-J. Hamsch, A. Moens, G. Sibbens, D. Vanleeuw, and M. Vidali, *Phys. Rev. C* **93**, 054603 (2016).
- [7] A. Oberstedt, R. Billnert, and S. Oberstedt, *Nucl. Instrum. Methods Phys. Res., Sect. A* **708**, 7 (2013).
- [8] S. Oberstedt, R. Billnert, A. Gatera, W. Geerts, P. Halipré, F.-J. Hamsch, M. Lebois, A. Oberstedt, P. Marini, M. Vidali, and J. N. Wilson, *Phys. Procedia* **64**, 83 (2015).
- [9] V. V. Verbinski, H. Weber, and R. E. Sund, *Phys. Rev. C* **7**, 1173 (1973).
- [10] A. Göök, F.-J. Hamsch, A. Oberstedt, and S. Oberstedt, *Nucl. Instrum. Methods Phys. Res., Sect. A* **664**, 289 (2012).
- [11] <https://root.cern.ch>.
- [12] S. Agostinelli *et al.* (Geant4 Collaboration), *Nucl. Instrum. Methods Phys. Res., Sect. A* **506**, 250 (2003).
- [13] J.-M. Régis, M. Dannhoff, J. Jolie, C. Müller-Gatermann, and N. Saed-Samii, *Nucl. Instrum. Methods Phys. Res., Sect. A* **811**, 42 (2016).
- [14] A. Chyzh, C. Y. Wu, E. Kwan, R. A. Henderson, J. M. Gostic, T. A. Bredeweg, A. Couture, R. C. Haight, A. C. Hayes-Sterbenz, M. Jandel, H. Y. Lee, J. M. O'Donnell, and J. L. Ullmann, *Phys. Rev. C* **87**, 034620 (2013).
- [15] O. Litaize and O. Serot, FIFRELIN ver. 2016 (private communication).
- [16] P. Talou, T. Kawano, I. Stetcu, J. P. Lestone, E. McKigney, and M. B. Chadwick, *Phys. Rev. C* **94**, 064613 (2016).
- [17] F. Pleasonton, *Nucl. Phys. A* **213**, 413 (1973).
- [18] J. L. Ullmann, E. M. Bond, T. A. Bredeweg, A. Couture, R. C. Haight, M. Jandel, T. Kawano, H. Y. Lee, J. M. O'Donnell, A. C. Hayes, I. Stetcu, T. N. Taddeucci, P. Talou, D. J. Vieira, J. B. Wilhelmy, J. A. Becker, A. Chyzh, J. Gostic, R. Henderson, E. Kwan, and C. Y. Wu, *Phys. Rev. C* **87**, 044607 (2013).
- [19] ENDF/B-VII.1 Evaluated Nuclear Data File ZA = 94239, MF = 15, MT = 18 (2011), <http://www.nndc.bnl.gov/exfor/endf00.jsp>.
- [20] M. Lebois, J. N. Wilson, P. Halipré, A. Oberstedt, S. Oberstedt, P. Marini, C. Schmitt, S. J. Rose, S. Siem, M. Fallot, A. Porta, and A.-A. Zakari, *Phys. Rev. C* **92**, 034618 (2015).